LAWRENCE
LIVERMORE
NATIONAL
LABORATORY

UCRL-JRNL-212536

Discrete Particle Noise in Particle-in-Cell Simulations of Plasma Microturbulence

W. M. Nevins, A. Dimits, G. Hammett

May 25, 2005

Physics of Plasmas

Discrete particle noise in particle-in-cell simulations of plasma microturbulence

W.M. Nevins and A. Dimits
Lawrence Livermore National Laboratory
Livermore, CA 94550

G. Hammett
Princeton Plasma Physics Laboratory
Princeton, NJ 08536

Abstract

Recent gyrokinetic simulations of electron temperature gradient (ETG) turbulence with flux-tube continuum codes vs. the global particle-in-cell (PIC) code GTC yielded different results despite similar plasma parameters. Differences between the simulations results were attributed to insufficient phase-space resolution and novel physics associated with toroidicity and/or global simulations. We have reproduced the results of the global PIC code using the flux-tube PIC code PG3EQ, thereby eliminating global effects as the cause of the discrepancy. We show that the late-time decay of ETG turbulence and the steady-state heat transport observed in these PIC simulations results from discrete particle noise. Discrete particle noise is a numerical artifact, so both these PG3EQ simulations and the previous GTC simulations have nothing to say about steady-state ETG turbulence and the associated anomalous heat transport. In the course of this work we develop three diagnostics which can help to determine if a particular PIC simulation has become dominated by discrete particle noise.

I. Introduction

Discrete particle noise in particle-in-cell (PIC) simulations of plasma microturbulence is an important issue which has been a major source of controversy between the PIC and continuum gyrokinetic simulation communities (see, for example, [Waltz, 2002; Candy, 2004]). Discrete particle effects in plasmas are associated with collisions, and generally decrease with increasing particle number. It is impractical to include as many particles in PIC simulation codes as are present in typical experimental plasmas, so PIC simulation codes seek to reduce discrete particle "noise" through the use of grids, smoothing (which is introduced while solving for the electro-magnetic fields), and finite-size particles. In addition, modern plasma microturbulence codes further reduce discrete particle effects by representing only the (small) departure of the particle distribution function from a Maxwellian [Dimits, 1993; Parker, 1993; Kotschenreuther, 1993]. A consequence of these noise reduction techniques is that the discrete particle effects which remain do not accurately reproduce collisional effects in the plasma being modeled, and must be viewed as numerical artifacts of the PIC (Monté Carlo like) integration technique. If the discrete particle noise does become important in a PIC simulation, then that simulation cannot be viewed as a faithful model of plasma microturbulence as it occurs in experimental plasmas.

Discrete particle noise is not just a notional problem in PIC simulations of plasma microturbulence. The work reported here began as an effort to understand the very different levels of heat transport reported in continuum [Dorland, 2000; Jenko, 2000; Jenko, 2002] and PIC [Lin, 2004; Lin, 2004a; Lin, 2005] simulations of electron temperature gradient (ETG) turbulence at nearly the same plasma parameters. The plasma parameters in question were originally used in the Cyclone ion temperature gradient (ITG) turbulence benchmarking effort [Dimits, 2000], so we will refer to this case as Cyclone base-case-like ETG turbulence. These very different simulation results have been variously attributed to insufficient phase-space resolution and/or an insufficient simulation volume [Lin, 2004; Lin, 2004a; Lin, 2005] in the simulations reported in Refs. [Dorland, 2000; Jenko, 2000; Jenko, 2002], and to novel physics associated with toroidicity and/or global simulation models [Lin, 2004; Lin, 2005]. We have reproduced the inverse cascade to long wave-length associated with the initial saturation, the late-time decay of the ETG turbulence, and the relatively low steady-state heat transport reported in Ref. [Lin, 2004; Lin, 2004a; Lin 2005] using the flux-tube PIC code, PG3EQ,[Dimits, 1996] thereby eliminating global effects as the source of the discrepancy between the ETG turbulence reported in Ref [Dorland, 2000; Jenko, 2000; Jenko, 2002] and Ref. [Lin, 2004; Lin, 2004a; Lin, 2005]. However, we will demonstrate that both the late-time decay of the ETG turbulence and the steady-state heat transport observed in our PG3EQ simulations and, by inference, in the GTC simulations reported in Ref. [Lin, 2004; Lin, 2004a; Lin, 2005] are a consequence of discrete particle noise. Hence, the PG3EQ simulations reported here and the GTC simulations reported in Ref. [Lin, 2004; Lin, 2004a; Lin, 2005] have nothing to say about steady-state heat transport associated with ETG turbulence in experimental plasmas.

These rather surprising results with respect to PIC simulations of ETG turbulence led us to revisit our analysis of Cyclone base case ITG turbulence. We conclude that discrete particle noise is also a factor in the longest Cyclone base case ITG turbulence simulations. This does not affect the results reported in Ref. [Dimits, 2000] because the simulations described in that paper terminated before discrete particle effects became important. However, it does affect related simulations, which have been reported at major meetings [Lee, 2004].

Fortunately, there is a literature on discrete particle noise [Langdon, 1979; Birdsall, 1985; Krommes, 1993; Hammett, 2005]. This literature allows us to quantify the level of discrete particle noise in any particular PIC simulation run, thereby casting the problem of discrete particle noise in PIC simulations as a code verification issue [Roache, 1998]. A major goal of this work is the development of diagnostics, described in Sec. III, which can be conveniently implemented in PIC simulations codes allowing retrospective verification of each simulation run.

II. Simulations of Cyclone base-case-like ETG turbulence

The Cyclone base case plasma parameters, which were originally introduced as a benchmark for simulations of ITG turbulence [Dimits, 2000], are $R_0/L_T=6.9$, $R_0/L_n=2.2$, $T_e/T_i=1.0$, $q=1.4$, and $s=(r/q)dq/dr=0.79$. These parameters have since been adopted in several numerical studies of ETG turbulence [Dorland, 2000; Jenko, 2000; Jenko, 2002; Lin, 2004, Lin, 2004a, Lin, 2005]. We revisit these plasma parameters in this study of Cyclone base-case-like ETG turbulence in an effort resolve the differences between Refs. [Dorland, 2000; Jenko, 2000; Jenko, 2002] and [Lin, 2004, Lin, 2004a, Lin, 2005].

The plasma parameters used for the Cyclone base-case-like ETG turbulence simulations reported in Ref. [Jenko, 2000; Jenko, 2002] differ from those considered in Ref. [Dorland, 2000; Lin, 2004, Lin, 2004a, Lin, 2005] in that Ref. [Jenko, 2000; Jenko, 2002] did not include magnetic trapping (since magnetic trapping is a finite-aspect-ratio effect, it can be eliminated by setting $r/R_0=0$), while Refs. [Dorland, 2000; Lin, 2004; Lin, 2004a; Lin, 2005] included magnetic trapping (by taking $r/R_0\approx0.18$). The inclusion of magnetic trapping makes only a small difference in the linear growth spectrum of ETG modes (see Fig. 1). However, this finite aspect-ratio effect is the only difference between the plasma parameters used in the simulations reported in Ref. [Jenko, 2000; Jenko, 2002] and those used in Ref. [Dorland, 2000; Lin, 2004; Lin, 2004a, Lin, 2005]. We investigate the effect of magnetically trapped electrons on Cyclone base-case-like ETG turbulence by comparing two sets of PG3EQ simulations, with ($r/R_0=0.18$) and without ($r/R_0=0$) magnetically trapped electrons.

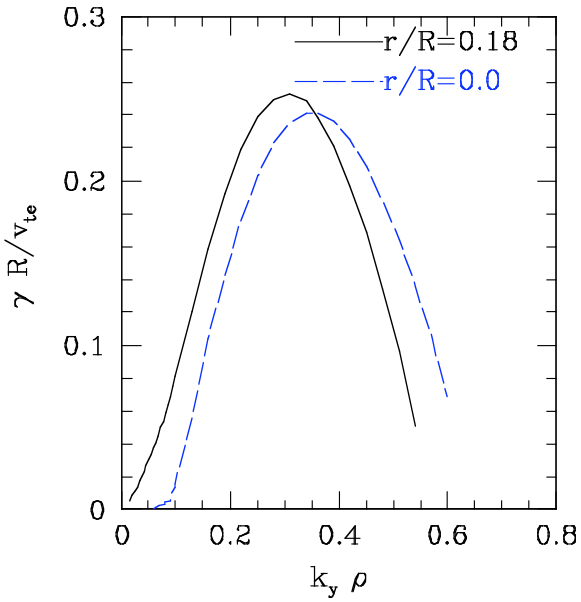

Figure 1. The linear growth rate for Cyclone base-case-like ETG modes is plotted vs. the wavenumber in the bi-normal direction, both with (black curve) and without (blue curve) magnetically trapped electrons.

II.1 Cyclone base-case-like ETG turbulence without magnetic trapping

We performed convergence studies in both particle number and flux-tube cross-section for Cyclone base-case-like ETG turbulence without magnetic trapping ($r/R_0=0$) using the flux-tube PIC code, PG3EQ[Dimits, 1996]. Figure 2 shows $\chi_e(t) \equiv Q_e(t)/\nabla T_0$ from this convergence study, where ∇T_0 is the equilibrium electron temperature gradient, $Q_e(t)$ is the radial electron heat flux, and the average is taken over the entire simulation volume. The particle number scan included runs at 2 particles/grid cell (blue curve in Fig. 2), 4 particles/grid cell (green curve in Fig. 2), 8 particles/grid cell (black curve in Fig. 2), and 16 particles/grid cell (red curve in Fig. 2). Convergence at late-times in flux-tube cross-section is demonstrated by comparing runs with a cross-section of $125\rho_e x 125\rho_e$ (128x128 grid cells with a grid spacing $\Delta x=\Delta y=0.9817\rho_e$), the blue, green, and black curves in Fig. 2, to a run with a cross-section of $250\rho_e x 62.5\rho_e$ (256x64 grid cells with the same grid spacing), the red curve in Fig. 2.

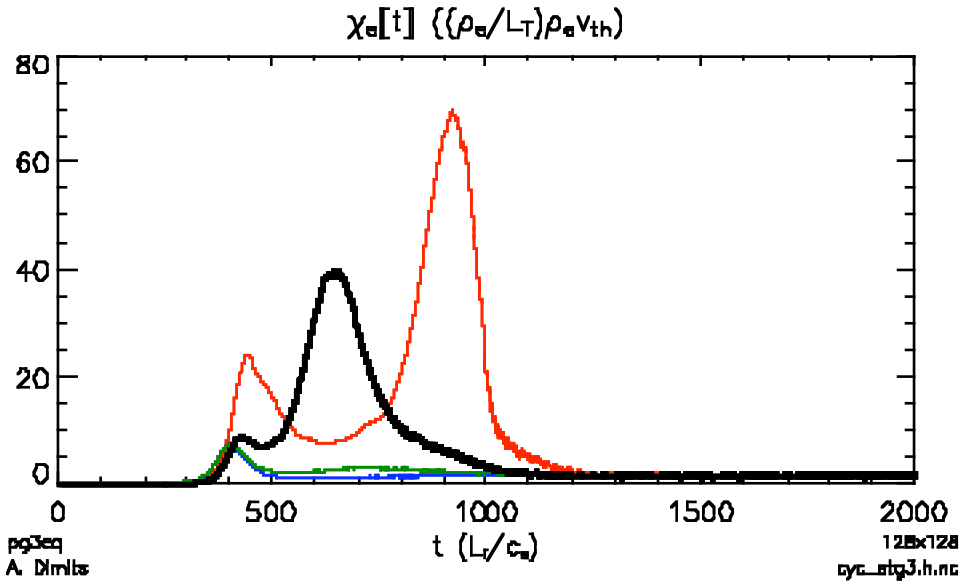

Figure 2. The coefficient of electron thermal transport, $\chi_e(t)$, from a particle-number and box-size convergence study of Cyclone base-case-like ETG turbulence without magnetic trapping ($r/R_0=0$) including runs in with a flux-tube cross-section of $125\rho_e x125\rho_e$ and 2 particles/grid cell (blue curve), 4 particles/grid cell (green curve), and 8 particles/grid cell (black curve); and a flux-tube cross-section of $250\rho_e x62.5\rho_e$ with 16 particles/grid cell (red curve).

In each simulation run there is a burst of ETG turbulence during which the instantaneous electron heat transport approaches, and often exceeds the transport level, $\chi_e \approx 13(\rho_e/L_T)\rho_e v_{te}$, reported in Ref. [Dorland, 2000; Jenko, 2000; Jenko, 2002]. Both the length and the amplitude of this burst increases with the number of particles per grid cell. However, at late times the turbulent heat transport in all of these simulations drops to an even lower level, $\chi_e \approx 1.5(\rho_e/L_T)\rho_e v_{te}$, than the late-time electron heat transport reported in Ref. [Lin, 2004; Lin, 2004a], $\chi_e \approx 3.2(\rho_e/L_T)\rho_e v_{te}$. The late-time electron heat transport in all of the PG3EQ simulations in our particle-number and box-size convergence study is nearly constant in time with $\chi_e \approx 1.5(\rho_e/L_T)\rho_e v_{te}$. Hence, the late-time (but not the intermediate time) $\chi_e \approx 1.5(\rho_e/L_T)\rho_e v_{te}$ from this study is converged in both particle number and box size.

In addition to exhibiting low heat transport at late times, these PG3EQ simulations exhibit the down-shift in perpendicular wave-number observed in Ref. [Lin]. Figure 3 shows the ETG fluctuation spectrum averaged over the radial variable (x) and plotted vs. $k_y\rho_e$ from a PG3EQ simulation with a cross-section of $125\rho_e x125\rho_e$ and 8 particles/grid cell (corresponding to the black curve in Fig. 2). Comparing the ETG fluctuation spectrum in the late linear phase, $t=420\ L_T/v_{te}$ (red curve in Fig. 3) to the fluctuation spectrum 20 linear growth times later at $t=995\ L_T/v_{te}$ (red curve in Fig. 3) we see a down-shift in the perpendicular wave number from $k_y\rho_e \approx 0.35$ in the linear phase to $k_y\rho_e \approx 0.15$ in the non-linear phase. This behavior is quite similar to that observed in Ref. [Lin, 2004;

Lin, 2004a, Lin, 2005] (*c.f.*, Fig. 1 of Ref [Lin, 2005]), despite the much smaller dimension of our flux-tube in the bi-normal direction ($125\rho_e$) and correspondingly large spacing ($\Delta k_y = 0.05/\rho_e$) between Fourier modes in k_y.

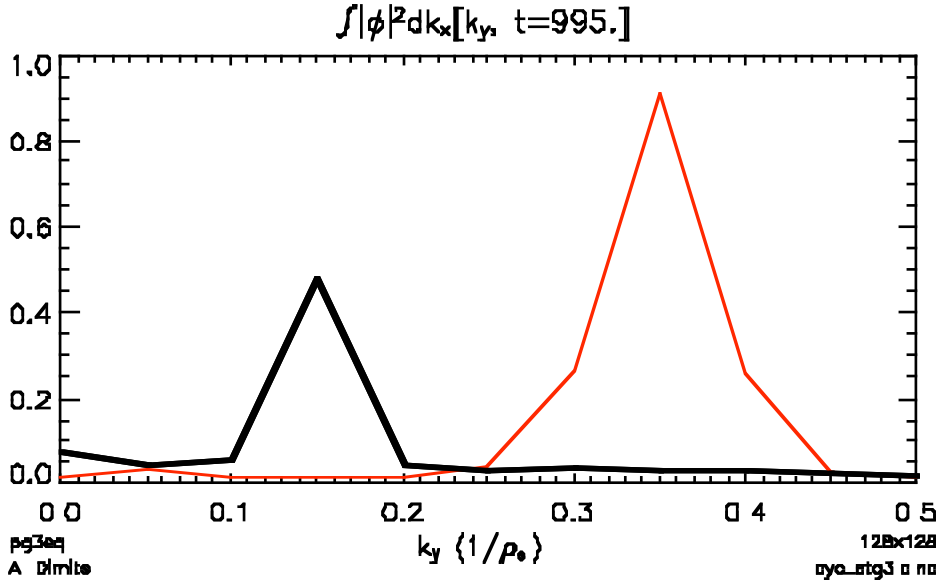

Figure 3. The ETG fluctuation spectra in the linear phase, $t=420\ L_T/v_{te}$ (red curve) and at $t\approx 20/\gamma$ after saturation from the PG3EQ simulation with a cross-section of $125\rho_e x 125\rho_e$ and 8 particles/grid cell (corresponding to the black curve in Fig. 2).

II.2 Cyclone base-case-like ETG turbulence with magnetic trapping

Concern about the radial box size relative to the radial correlation length of the ETG "streamers" led us to substantially increase the flux-tube cross-section in our PG3EQ simulations of Cyclone base-case-like ETG turbulence with magnetic trapping ($r/R_0=0.18$). However, neither the increase in flux-tube cross-section nor the inclusion of magnetic trapping made a qualitative change in our simulation results. Figure 4 shows a convergence study in particle number and flux-tube cross-section of Cyclone base-case-like ETG turbulence simulations. The particle number scan included runs with 2 particles/grid cell (green curve in Fig. 4), 4 particles/grid cell (blue curve in Fig. 4), and 16 particles/grid cell (red curve in Fig. 4). In these runs the flux-tube cross-section is held fixed at $500\rho_e x 125\rho_e$ (512 grid cells in the radial direction and 128 cells in the bi-normal direction). Convergence in flux-tube cross-section is demonstrated by comparing the late-time values of $\chi_e(t)$ from this particle-number convergence study with $\chi_e(t)$ from a simulation with a flux tube cross-section of $250\rho_e x 62.5\rho_e$ (256x64 grid cells) shown by the black curve in Fig. 4. In every case there is a burst of ETG turbulence accompanied by substantial electron heat transport. As before, the duration and amplitude of the burst

of ETG turbulence increases with the number of particles per grid cell. At late times both the fluctuation intensity and the heat transport drop to a low level. The late-time electron heat transport observed in Cyclone base-case-like ETG simulations with magnetic trapping is also independent of the number of particles per grid cell or of the simulation cross-section. Quantitatively, we find $\chi_e \approx 3(\rho_e/L_T)\rho_e v_{te}$, in excellent agreement with the heat transport reported by Ref. [Lin, 2004; Lin, 2004a] , $\chi_e \approx 3.2(\rho_e/L_T)\rho_e v_{te}$.

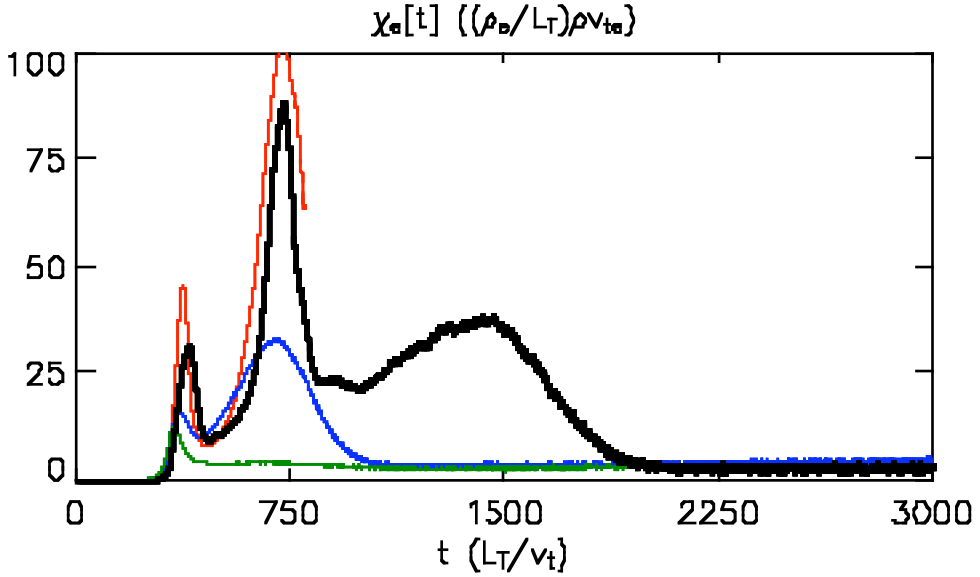

Figure 4. The coefficient of electron thermal transport, $\chi_e(t)$, from a particle-number and flux tube cross-section convergence study of Cyclone base-case-like ETG turbulence with magnetic trapping ($r/R_0=0.18$), including runs in a flux-tube with cross-section $500\rho_e x125\rho_e$ with 2 particles/grid cell (green curve), 4 particles/grid cell (blue curve), and 16 particles/grid cell (red curve); and a flux-tube cross-section of $250\rho_e x62.5\rho_e$ with 16 particles/grid cell.

In addition to reproducing the heat transport reported by Ref. [Lin, 2004; Lin, 2004a], we reproduce the inverse cascade wave-number. Figure 5 shows the fluctuation spectrum averaged over the radial variable (x) and plotted vs. $k_y\rho_e$ in the linear phase, $t=400\ L_T/v_{te}$ (red curve in Fig. 5) and at a time $30/\gamma_0 \approx 828\ L_T/v_{te}$ after the initial saturation of the ETG turbulence. The PG3EQ simulation again reproduces the downshift in the perpendicular wave-number described in the global simulations of Ref. [Lin, 2004: Lin, 2004a; Lin, 2005] (c.f., Fig. 1 of Ref. [Lin, 2005]) despite the much smaller dimension of our flux-tube in the bi-normal direction ($62.5\rho_e$) and correspondingly large spacing ($\Delta k_y = 0.1/\rho_e$) between Fourier modes in k_y.

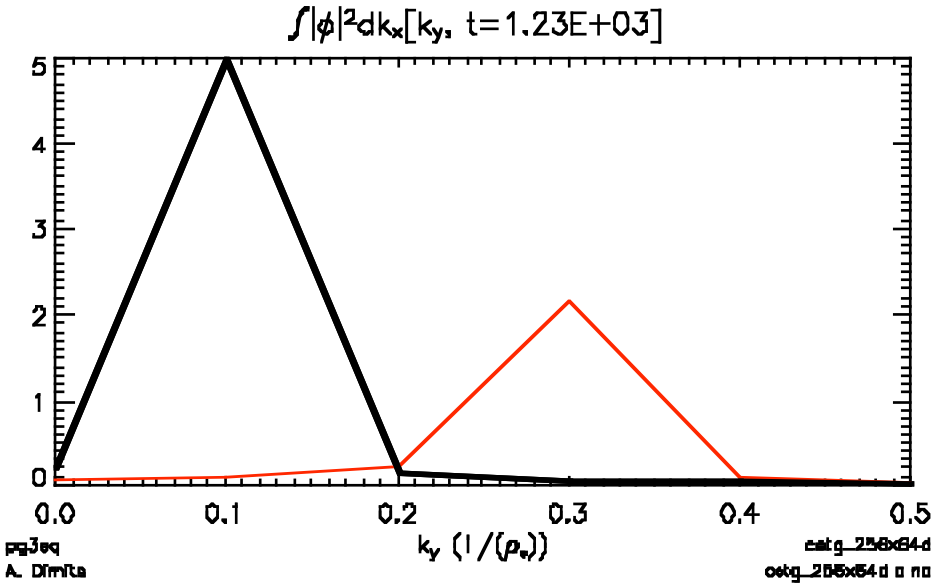

Figure 5. . The ETG fluctuation spectra in the linear phase, $t=400\ L_T/v_{te}$ (red curve) and at 30 linear growth times later at $t\approx 1228\ L_T/v_{te}$. Data from the PG3EQ simulation with a cross-section of $250\rho_e x 62.5\rho_e$ and 16 particles/grid cell (corresponding to the black curve in Fig. 4).

II.3 Late-time ETG potential fluctuations

An examination of Figs. 2 through 5 leads one to conclude that our PG3EQ simulations are converged in both particle number and systems size. It would seem to follow that steady-state Cyclone base-case-like ETG turbulence produces very little heat transport, in agreement with Ref. [Lin, 2004; Lin, 2004a] and in contradiction to Ref. [Dorland, 2000; Jenko, 2000; Jenko, 2002]. However, an examination of the late-time potential fluctuations in our simulations of Cyclone base-case-like ETG turbulence indicates that this conclusion is unwarranted.

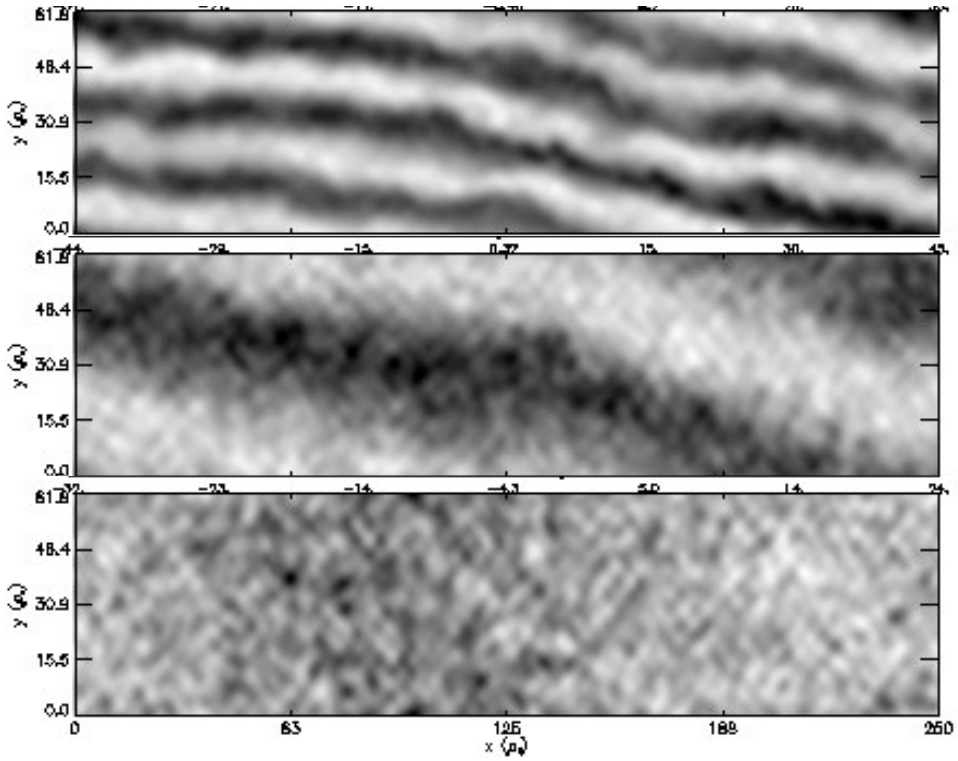

Figure 6. Contour plots of the potential on the outboard mid-plane at $t=400\ L_T/v_{te}$ during the linear phase (top panel) and 30 linear growth times later at $t=1228\ L_T/v_{te}$ (middle panel) show the characteristic ETG "streamers". These streamers are absent at very late times, $t=2500\ L_T/v_{te}$ (bottom panel) during the steady-state phase of the PG3EQ simulation of Cyclone base-case-like ETG turbulence.

Figure 6 shows a contour plot of the mid-plane potential fluctuations both during the burst of ETG turbulence and at late times during the "steady-state" period where particle number and flux-tube cross-section convergence were achieved. It is immediately obvious from Fig. 6 that the late-time potential fluctuations have little in common with the characteristic, large-scale ETG "streamers" seen during the earlier burst of ETG turbulence when the electron heat transport was large. There are no large-scale potential

structures at late times in our PG3EQ simulations of Cyclone base-case-like ETG turbulence. Instead, the grey-tone rendering in Fig. 6 of the late-time potential fluctuations looks rather like the image on the screen of a TV set whose antenna has been disconnected. Since the late-time potential looks like shot-noise, we were led to investigate the hypothesis that the late-time behavior of our PG3EQ simulations, and (by inference) the GTC simulations described in Ref. [Lin, 2004; Lin, 2004a; Lin, 2005] are dominated by discrete particle noise.

III. Discrete Particle Noise

There is an extensive literature to draw upon when quantifying discrete particle noise. The treatment below loosely follows Chp. 12 of Ref. [Birdsall, 1985]. We begin with the Fourier-space representation of the gyrokinetic Poisson equation [Lee, 1983]:

$$\left\{1+\left[1-\Gamma_0(k_\perp^2\rho_e^2)\right]\right\}\frac{e\phi_k}{T}=\frac{S_{filter}(\mathbf{k})}{N_p}\sum_i w_i J_o(k_\perp\rho_i)\exp(-i\mathbf{k}\cdot\mathbf{x}_i) \qquad (1)$$

where the first term on the left-hand-side (LHS) represents Debye shielding (by ions in the case of ETG turbulence), while the term in square brackets on the LHS represents the polarization of the kinetic electron species. The right-hand-side (RHS) includes any spatial filtering applied to the electrostatic potential, $S_{filter}(\mathbf{k})$, the total number of simulation particles, N_p, the individual particle weights, w_i, and the Bessel function, $J_0(k_\perp\rho_i)$, where ρ_i is the gyro-radius of the i^{th} electron. This equation is easily solved for the electrostatic potential:

$$\frac{e\phi_{\mathbf{k}}}{T}=\frac{S_{filter}(\mathbf{k})}{N_p\left[2-\Gamma_0(k_\perp^2\rho_e^2)\right]}\sum_i w_i J_o(k_\perp\rho_i)\exp(-i\mathbf{k}\cdot\mathbf{x}_i)\ . \qquad (2)$$

Squaring this expression, we obtain the spectral density,

$$\left\langle\left|\frac{e\phi_{\mathbf{k}}}{T}\right|^2\right\rangle_N=\frac{S_{filter}^2(\mathbf{k})}{\left[2-\Gamma_0(k_\perp^2\rho_e^2)\right]^2}\left[\frac{1-\Gamma_0(k_\perp^2\rho_e^2)\left\langle w^2\right\rangle}{N_p}+\frac{1}{N_p^2}\left\langle\sum_{i\neq j} w_i w_j J_0(k_\perp\rho_i)J_0(k_\perp\rho_j)\exp\left[-i\mathbf{k}\cdot(\mathbf{x}_i-\mathbf{x}_j)\right]\right\rangle\right] \qquad (3)$$

where both i and j index computer particles, and the average is to be taken over an ensemble of realizations of the computer particles. The second term on the RHS represents correlations between computer particle positions and weights. This term describes the contribution of waves, instabilities, and turbulence to the spectral density. We can isolate the contribution of discrete particle noise by ignoring correlations among the computer particle positions and weights. The second term on the RHS then vanishes, and we are left with the fully uncorrelated fluctuation spectrum,

$$\left\langle \left| \frac{e\phi_{\mathbf{k}}}{T} \right|^2 \right\rangle_N = \frac{\langle w^2 \rangle S_{filter}^2(\mathbf{k}) \Gamma_0(k_\perp^2 \rho_e^2)}{N_p \left[2 - 2\Gamma_0(k_\perp^2 \rho_e^2) \right]^2} \quad (\mathbf{k} \neq 0) \quad \frac{\langle w^2 \rangle}{N_p} \tag{4}$$

In the limit $|\mathbf{k}| \to 0$, the fully uncorrelated spectrum goes to the mean-squared particle weight, $\langle w^2 \rangle$ divided by the number of simulation particles.

It is our experience that the fully uncorrelated spectrum overstates the discrete particle noise at low k by up to a factor of 2. A more complete derivation of discrete particle noise, which includes the effects of self-Debye shielding by the kinetic species, may be found in Ref. [Hammett, 2005]. When the self-Debye shielding is included, our estimate of the spectrum of discrete particle noise is reduced to

$$\left\langle \left| \frac{e\phi_{\mathbf{k}}}{T} \right|^2 \right\rangle_H = \frac{\langle w^2 \rangle S_{filter}^2(\mathbf{k}) \Gamma_0(k_\perp^2 \rho_e^2)}{N_p \left[2 - 2\Gamma_0(k_\perp^2 \rho_e^2) \right] \left[2 - \left(1 - S_{filter}(\mathbf{k}) d_\parallel(\mathbf{k}) \right) \Gamma_0(k_\perp^2 \rho_e^2) \right]} \quad (\mathbf{k} \neq 0) \quad \frac{\langle w^2 \rangle}{2N_p} \tag{5}$$

where $d_{||}(\mathbf{k})$ is related to k-space representation of the differencing operator used to obtain the parallel electric field from the potential. In the limit of large-$k_\perp$, the term $S_{filter}(\mathbf{k}) d_{||}(\mathbf{k})$ vanishes and these two estimates of the discrete particle noise spectrum are identical. The effect of including self-Debye shielding is to reduce the estimate of the discrete particle fluctuation level by a factor of 2 at small k.

Examining Eqs. (4) and (5), we see that our estimates of the noise spectrum depend only on the numerical algorithms used in the field solve [which determine $S_{filter}(\mathbf{k})$, $\Gamma_0(k_\perp^2 \rho_{th}^2)$, and $d_{||}(\mathbf{k})$], and the mean-squared particle weight, $\langle w^2 \rangle$. The mean-squared particle weight has the interesting property that it is monotonically increasing in time. This follows from the entropy theorem of Lee and Tang [Lee , 1988], which relates the rate of increase in $\langle w^2 \rangle$ to the heat flux:

$$\frac{d\langle w^2 \rangle}{dt} \propto \frac{2\Gamma_e(t)}{L_T^2} \tag{6}$$

Particle-in-cell simulation codes compute and save $\langle w^2 \rangle$ as a function of time as the simulation progresses. Hence all the information required to evaluate either of our estimates of the discrete particle noise spectrum is available.

Typically, only a limited amount of fluctuation data is retained in simulations of plasma microturbulence. In the simulations described in Sec. II above we only retained the time history of the potential at the outboard midplane (labeled $z = 0$ in PG3EQ's coordinate system). This allows us to compute the fluctuation spectrum at $z=0$, which must be compared with a mixed (Fourier and configuration-space) representation of the discrete particle noise spectrum,

$$\left\langle \left| \frac{e\phi_{k_x,k_y}(z)}{T} \right|^2 \right\rangle = \sum_{k_z} \left\langle \left| \frac{e\phi_{k_x,k_y,k_z}}{T} \right|^2 \right\rangle$$
$$\frac{\left\langle w^2 \right\rangle}{n_p \left(L_x L_y \Delta z \right)} \left[\frac{\Delta z}{2\pi} \int_{-\pi/\Delta z}^{\pi/\Delta z} \frac{S_{filter}^2 \Delta_0}{\left[2\left(1 - \Delta_0 \right) \right] \left[2\left(1 - S_{filter} d_{\parallel} \right) \Delta_0 \right]} dk_z \right] \tag{7}$$

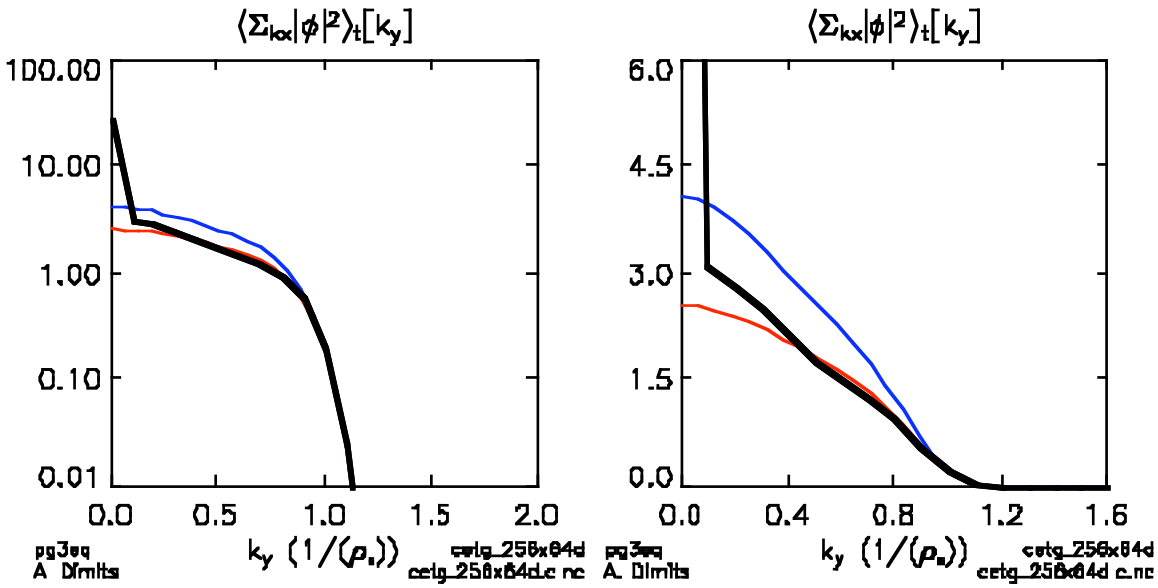

Figure 7. (a) The fluctuation spectrum at the outboard midplane averaged over the radial coordinate (x) and the interval $2500\ L_T/v_{te} < t < 3000\ L_T/v_{te}$ is plotted on a semi-log scale vs. k_y (black curve), together with the corresponding fully unshielded noise estimate (blue curve) and self-Debye shield noise estimate (red curve). (b) Same data on a linear scale.

In Figure 7 we compare the predicted noise spectrum plotted vs. $k_y\rho_e$ to the late-time fluctuation spectrum from the $250\rho_e x 62.5\rho_e$ (256x64 grid cells) PG3EQ simulation of Cyclone base-case-like ETG turbulence with magnetic trapping ($r/R_0=0.18$) shown in Figs. 4, 5, and 6. The spectrum has been averaged over both the radial coordinate and time ($2500\ L_T/v_{te} < t < 3000\ L_T/v_{te}$). In Figure 8 we compare the predicted noise spectrum plotted vs. vs. $k_x\rho_e$ to the late-time fluctuation spectrum from the same data set averaged over the bi-normal coordinate (y). The spectra shown in Figs. 7 and 8 differ largely because the field-solve in PG3EQ is asymmetric. Fourier techniques are use in the bi-normal (y) direction, while finite difference techniques are used in the radial (x) direction. In both Figs. 7 and 8 there is good agreement between the observed late-time fluctuation spectrum and the fully-uncorrelated noise spectrum; while there is excellent agreement with the self-Debye shielded noise spectrum. The only significant feature seen in the signal and not iin our prediction of the discrete particle noise spectrum is a zonal flow ($k_x\rho_e=0.025$, $k_y\rho_e=0$), which does not contribute to radial transport. We conclude from this that the PG3EQ Cyclone base-case-like ETG turbulence simulations

described in Sec. II are dominated by discrete particle noise at late times; and that the estimates of the discrete particle noise given above in Eqs. (4) and (5) accurately reproduce the fluctuation spectrum observed in PIC simulations which are dominated by discrete particle noise.

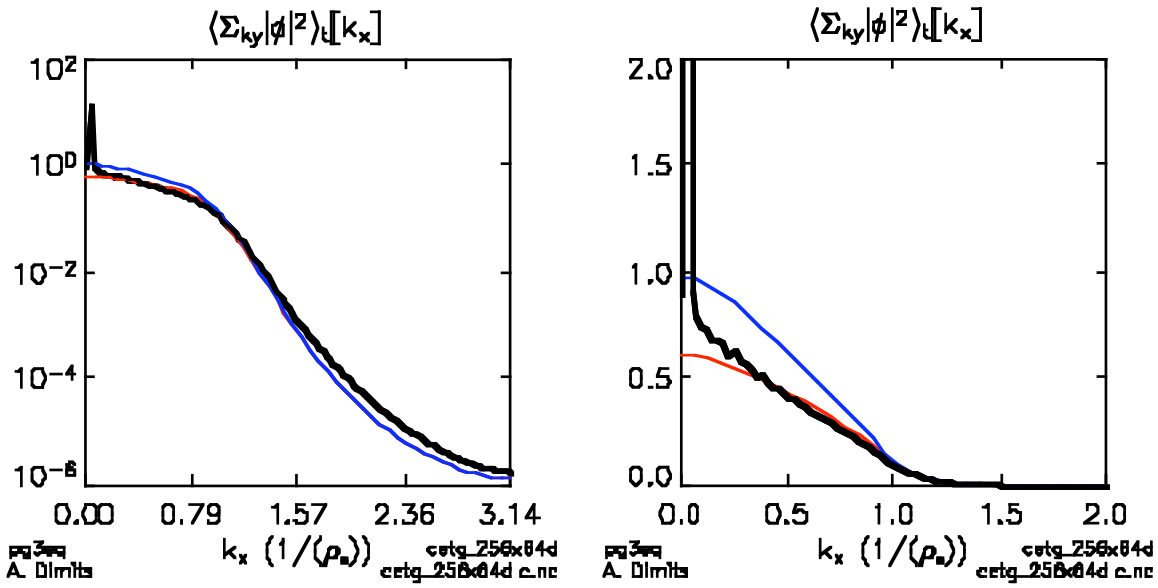

Figure 8. a) The fluctuation spectrum at the outboard midplane averaged over the bi-normal coordinate (y) and the interval $2500\ L_T/v_{te} < t < 3000\ L_T/v_{te}$ is plotted on a semi-log scale vs. k_x (black curve), together with the corresponding fully unshielded noise estimate (blue curve) and self-Debye shield noise estimate (red curve). (b) Same data on a linear scale.

Comparisons between the observed fluctuation spectrum and the predicted noise spectrum provide a means of determining when a particular simulation run is dominated by discrete particle noise. However, this diagnostic is computationally intensive and requires the retention of substantial amounts of simulation data. A less computationally intensive diagnostic involves comparing the observed fluctuation intensity, $\langle |e\phi/T|^2 \rangle$, with the fluctuation intensity expected from discrete particle noise alone,

$$\left\langle \left| \frac{e\phi}{T} \right|^2 \right\rangle = \sum_{\mathbf{k}} \left\langle \left| \frac{e\phi_{\mathbf{k}}}{T} \right|^2 \right\rangle = \frac{\langle w^2 \rangle}{n_p V_{shield}} \tag{8}$$

where n_p is the number density of computer particles, the fully uncorrelated shielding volume is given by

$$V_{shield}^{(N)} \equiv \left[\frac{1}{(2\pi)^3} \int d^3\mathbf{k} \frac{S_{filter}^2 \varepsilon_0 (k^2 \lambda_e^2)}{\left[2 \varepsilon_0 (k^2 \lambda_e^2) \right]^2} \right]^{-1} \tag{9}$$

while the self-Debye shielded volume is given by

$$V_{shield}^{(H)} \equiv \left[\frac{1}{(2\pi)^3} \int d^3\mathbf{k} \frac{S_{filter}^2 \varepsilon_0 (k_\perp^2 \lambda_e^2)}{\left[2 - \varepsilon_0 \right] \left[2 - \left(1 - S_{filter} d_\parallel \right) \varepsilon_0 \right]} \right]^{-1} \tag{10}$$

Alternatively, one can construct the fluctuation energy density,

$$\tfrac{1}{2} m \left\langle V_{ExB}^2 \right\rangle = \left(\frac{\omega_p^2}{\Omega_c^2} \right) \left\langle \frac{\left| \delta \phi \right|^2}{4\pi} \right\rangle \tag{11}$$

This has direct physical significance (the kinetic energy associated with the *ExB* motion), and is closely related to the transport coefficient, $D \approx \left| V_{ExB} \right|^2 \tau_{corr}$. The contribution of the discrete particle noise to the fluctuation energy density is

$$\left(\frac{\omega_p^2}{\Omega_c^2} \right) \left\langle \frac{\left| \delta \phi \right|^2}{4\pi} \right\rangle = nT \frac{\left\langle w^2 \right\rangle}{n_p V_{shield}} \left\langle K_\perp^2 \left| \delta \right|^2 \right\rangle_{noise} \tag{12}$$

where expressions for V_{shield} are given above. The average over the discrete particle noise spectrum of the perpendicular wave vector is given by

$$\left\langle K_\perp^2 \left| \delta \right|^2 \right\rangle_{noise}^{(N)} \equiv \left[\frac{V_{shield}}{(2\pi)^3} \int d^3\mathbf{k} \frac{K_\perp^2(\mathbf{k}) \left| \delta \right|^2 S_{filter}^2(\mathbf{k}) \varepsilon_0 (k_\perp^2 \lambda_e^2)}{\left[2 - \varepsilon_0 (k_\perp^2 \lambda_e^2) \right]^2} \right] \tag{13}$$

for the fully uncorrelated noise spectrum, and by

$$\left\langle K_\perp^2 \left| \delta \right|^2 \right\rangle_{noise}^{(H)} \equiv \left[\frac{V_{shield}}{(2\pi)^3} \int d^3\mathbf{k} \frac{K_\perp^2(\mathbf{k}) \left| \delta \right|^2 S_{filter}^2(k) \varepsilon_0 (k_\perp^2 \lambda_e^2)}{\left[2 - \varepsilon_0 \right] \left[2 - \left(1 - S_{filter} d_\parallel \right) \varepsilon_0 \right]} \right] \tag{14}$$

for the self-Debye shielded noise spectrum.

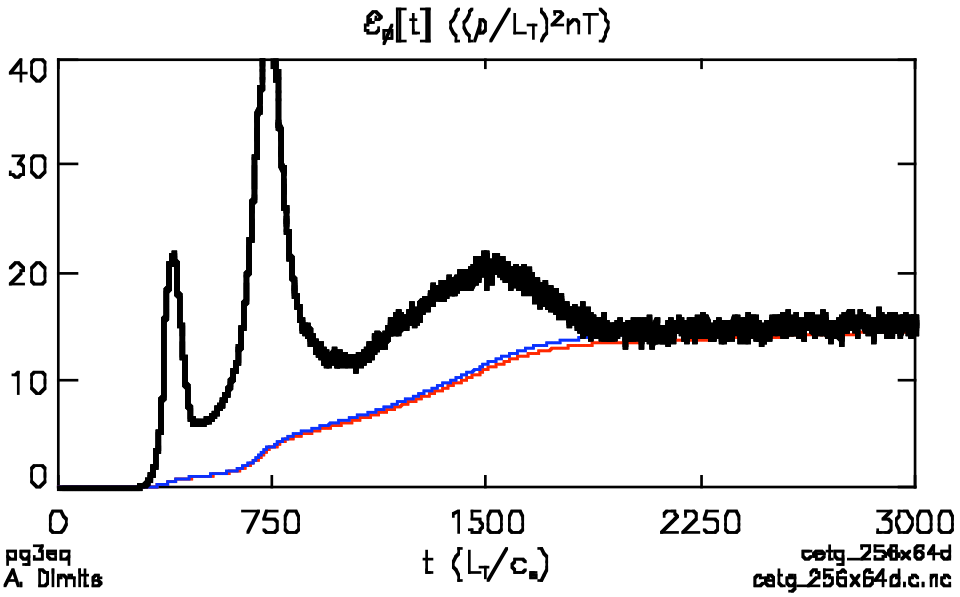

Figure 9. The fluctuation energy averaged over the outboard midplane (black curve) is compared to the fluctuation intensity from the fully uncorrelated noise spectrum (blue curve) or self-Debye shielded noise spectrum (red curve).

In figure 9 we compare our estimates of the fluctuation energy to that observed at the outboard mid-plane in the $250\rho_e x 62.5\rho_e$ (256x64 grid cells) PG3EQ simulation of Cyclone base-case-like ETG turbulence with magnetic trapping ($r/R_0=0.18$) shown in Figs. 4, 5, 6, 7, and 8. This diagnostic make it clear that (1) this simulation is dominated by discrete particle noise for $t > 1000\ L_T/v_{te}$ in the sense that more than half of the fluctuation energy can be accounted for by discrete particle noise; and (2) essentially all of the fluctuation energy can be accounted for by discrete particle noise for $t > 2000\ L_T/v_{te}$.

Figure 9 illustrates that PIC simulation of Cyclone base-case-like ETG turbulence is a pathological case in the sense that the ETG turbulences dies away at late-times, leaving only the discrete particle noise. This makes it difficult to develop a useful rule-of-thumb to use when evaluating the discrete particle noise diagnostics developed in this section. Fortunately, we have other examples of discrete particle noise in PIC simulations. In figure 10 we compare the observed fluctuation energy from both PG3EQ and GTC simulations Cyclone base-case ITG turbulence to the noise estimates. The drop in χ_i at late times ($t>500\ a/c_s$) occurs as the energy associated with the discrete particle fluctuations exceeds half of the total fluctuation energy. This suggests that, as a rule-of-thumb, we consider a PIC simulation to be dominated discrete particle noise when more than 1/2 of the total fluctuation energy can be attributed to discrete particle noise.

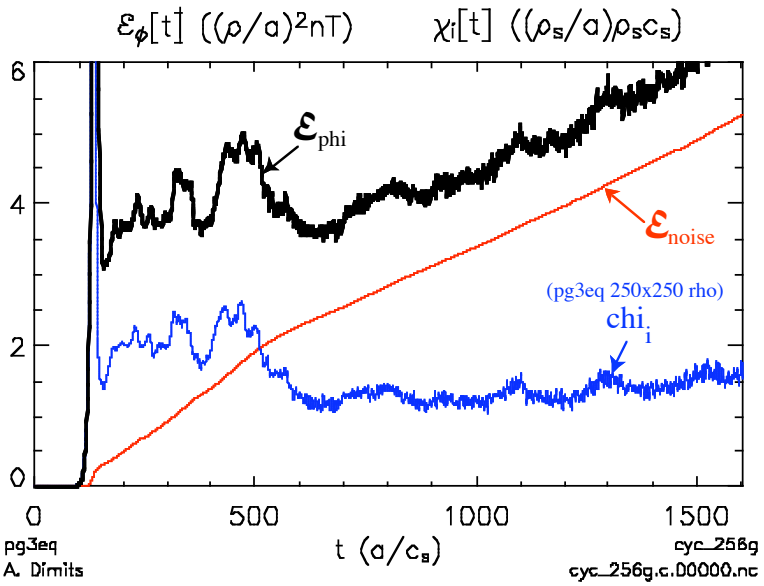

Figure 10. The fluctuation energy is plotted vs. time for a PG3EQ simulation of Cyclone base-case ITG turbulence (black curve). The red curve shows the fluctuation energy expected from the discrete particle noise. The corresponding level of thermal transport from this PG3EQ simulation is shown by the blue curve.

IV. Can discrete particle noise suppress ETG turbulence?

We demonstrated in Sec. III that our PG3EQ simulations of Cyclone base-case-like ETG turbulence are dominated by discrete particle noise at late-times. However, this does not occur due to the discrete particle noise rising to engulf the ETG signal. Instead, the ETG turbulence dies away, leaving the discrete particle noise behind (see Fig. 9). This raises the question of why the ETG turbulences died off. The particle-number convergence studies illustrated in Figs. 2 and 4 provide a clue. According to Eqs. (8) and (12) intensive measures of discrete particle noise, like the fluctuation intensity or the fluctuation energy density, decrease when the number of particles per grid cell is increased. Hence, we might have expected both the late-time fluctuation level and the heat transport to decrease with increasing particle number in these. Instead, both the late-time fluctuation level and electron heat transport are independent of the particle number, while the duration of the initial burst of ETG turbulence increases with increasing particle number. This suggests that there is a critical level of an intensive measure of discrete particle noise [like the intensity or energy density of the noise fluctuations as defined in Eqs. (8) and (12)] which suppresses the ETG turbulence. Increasing the number of simulation particles reduces the rate at which intensive measures of discrete particle noise grow (explaining the increase in the duration of the initial burst of ETG turbulence with increasing particle number), while the late-time electron heat transport is determined by

the noise level required to suppress the ETG turbulence (explaining why the late-time heat transport is independent of the particle number).

We investigate the hypothesis that discrete particle noise can suppress ETG turbulence using the "noise test" of Lin and Bolton [Lin, 2005a]. We implement the noise test by selecting a reference PG3EQ simulation of Cyclone base-case-like ETG turbulence from the flux-tube cross-section convergence study with magnetic trapping ($r/R_0=0.18$) illustrated in Fig. 4. We consider the case with a flux-tube cross-section $250\rho_e$x$62.5\rho_e$ (256x64 grid cells). Like the other simulations illustrated in Fig. 3, the late-time behavior of this simulation was dominated by discrete particle noise. When this simulation ended at $t=3000\ L_T/v_{te}$ the mean-squared particle weight was $\delta w^2_{final} \approx 7.85 \times 10^{-4}\ (\rho_e/L_T)$. If our hypothesis is correct, this mean-squared particle weight should, by itself, be sufficient to suppress Cyclone base-case-like ETG turbulence. The "noise test" investigates this hypothesis by re-initializing the simulation with all parameters set as they were at the beginning of the reference simulation except for the mean-squared particle weight. The initial weights of individual particles are then chosen from a random distribution scaled such that the means-square weight, $\delta w^2_{initial}$, is proportional to the final mean-squared particle weight from our reference simulation, δw^2_{final}. In electrostatic δf PIC simulations, any "memory" of past events is encoded into the particle phase variables, so this test effectively erases all memory of the previous burst of ETG turbulence other than the discrete particle noise level as quantified by the mean-squared particle weight.

Figure 11 shows the result when we re-initialized this simulation with $\delta w^2_{initial} = \delta w^2_{final}$ (red curve), $\delta w^2_{initial} = (1/2)\ \delta w^2_{final}$ (blue curve), $\delta w^2_{initial} = (1/4)\ \delta w^2_{final}$ (green curve), $\delta w^2_{initial} = (1/8)\ \delta w^2_{final}$ (chartreuse curve), $\delta w^2_{initial} = (1/16)\ \delta w^2_{final}$ (gold curve). When the simulation is restarted with $\delta w^2_{initial} = \delta w^2_{final}$ (red curve in Fig. 11), χ_e rises to the value it had at the end of the reference run [$\chi_e \approx 3\ (\rho_e/L_T)\rho_e v_{te}$] over a time interval of $2.5\ L_T/v_{te}$ (this short time interval is too short to be resolved in Fig. 11), and stays at approximately this value over the remainder of the simulation (an time interval of about $1000\ L_T/v_{te}$). The behavior of the restart with $\delta w^2_{initial} = (1/2)\ \delta w^2_{final}$ (blue curve if Fig. 10) is similar. The electron heat flux, measured by χ_e, now rises to a somewhat lower value [$\chi_e \approx 2\ (\rho_e/L_T)\rho_e v_{te}$] over the initial time interval of $2.5\ L_T/v_{te}$, and stays at approximately that value over the remainder of the simulation. While some low-level potential fluctuations with real frequencies satisfying the linear dispersion relation of the ETG modes are present after the restart in these runs, they have no apparent effect on the observed electron heat transport.

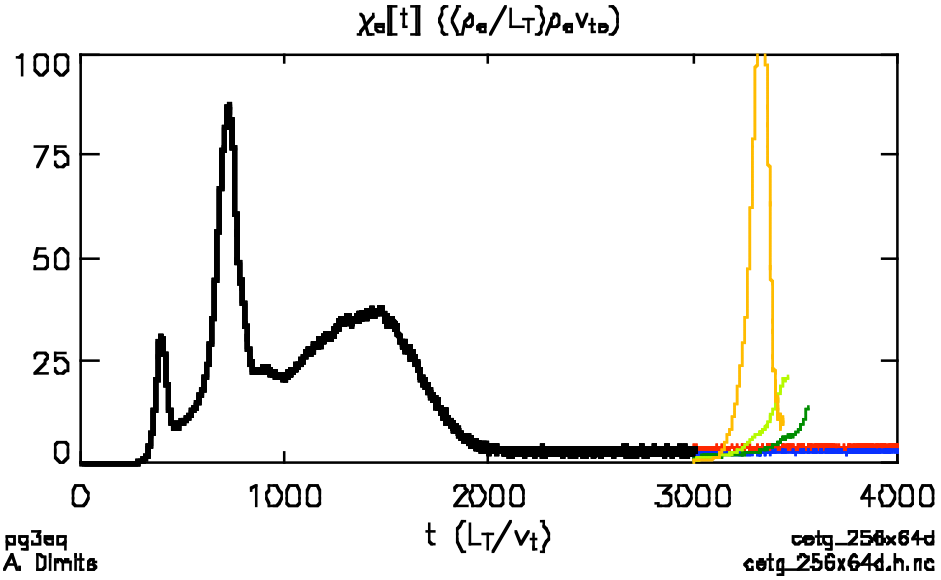

Figure 11. Electron heat flux from the "Noise Test" of Lin and Bolton. The black curve is from the initial simulation. The remaining 5 curves correspond to simulations initialized with $\delta w^2_{initial} = \delta w^2_{final}$ (red curve), $\delta w^2_{initial}=(1/2)\ \delta w^2_{final}$ (blue curve), $\delta w^2_{initial}=(1/4)\ \delta w^2_{final}$ (green curve), $\delta w^2_{initial}=(1/8)\ \delta w^2_{final}$ (chartreuse curve), $\delta w^2_{initial}=(1/16)\ \delta w^2_{final}$ (gold curve).

When the restart is initialized with progressively lower mean-squared particle weights the electron heat transport initially rises to progressively lower values: for $\delta w^2_{initial}=(1/4)\ \delta w^2_{final}$ (green curve in Fig. 9) χ_e rises to about $1.2\ (\rho_e/L_T)\chi_e v_{te}$ over the initial time interval; for $\delta w^2_{initial}=(1/8)\ \delta w^2_{final}$ (chartreuse curve in Fig. 9) χ_e rises to about $0.7\ (\rho_e/L_T)\chi_e v_{te}$ over the initial time interval; and for $\delta w^2_{initial}=(1/16)\ \delta w^2_{final}$ (gold curve in Fig. 9) χ_e rises to about $0.25\ (\rho_e/L_T)\chi_e v_{te}$ over the initial time interval. However, χ_e is no longer approximately constant over the remainder of the run. Instead, the we see linear growth of ETG modes accompanied by a pronounced rise in χ_e after the restart. The measured linear growth rates of ETG modes and the maximum in χ_e during the initial burst of ETG turbulence increase with decreasing $\delta w^2_{initial}$.

We conclude from this noise test that discrete particle noise can suppress ETG turbulence and the associated anomalous electron heat transport. The critical value of the mean-squared particle weight required to suppress Cyclone base-case-like ETG turbulence, δw^2_{crit} lies within the interval $0.25\ \delta w^2_{final} < \delta w^2_{crit} < 0.5\ \delta w^2_{final}$.

V. Summary and Conclusions

We have quantitatively reproduced key results from GTC simulations of Cyclone base-case-like ETG turbulence, including both the evolution of the turbulent ETG spectrum toward from an initial peak near $k_\perp \rho_e \approx 0.3$ in the linear phase of the simulation to $k_\perp \rho_e \approx 0.1$ in the nonlinear phase and the low steady-state electron heat transport, $\chi_e \approx 3\,(\rho_e/L_T)\,\rho_e v_{te}$, at late times in these simulations.

These simulations begin with linear growth of ETG modes, followed by a burst of ETG turbulence which dies away at late times, accounting for the low steady-state rate of electron heat transport. We find that the late-time fluctuation spectrum of our PG3EQ simulations and, by inference, the GTC simulations we have reproduced are dominated by discrete particle noise. Discrete particle noise is a numerical artifact of the Monté Carlo nature of the PIC simulation method. Hence, the late-time behavior of both the PG3EQ simulations reported here, and the GTC simulations reported in Ref. [Lin], does not model ETG turbulence as it occurs in experimental plasmas.

At earlier times, during the initial burst of ETG turbulence, we find that both the intensity of the ETG turbulence and the magnitude of the electron heat transport increases with increasing numbers of simulation particles per grid cell. Since similar numbers of simulation particles/grid cell were employed both in our PG3EQ simulations and in GTC simulations we reproduced, we conclude that neither our PG3EQ simulations nor the GTC simulations which we have reproduced were converged in particle number during the burst of ETG turbulence which occurred before these simulations became dominated by discrete particle noise. Hence, neither the PG3EQ simulations of Cyclone base-case-like ETG turbulence, nor the GTC simulations we have reproduced, have anything to say about the anomalous electron heat transport associated with ETG turbulence in experimental plasmas.

We also demonstrate that discrete particle noise at the level observed at late times in these simulations is sufficient to suppress both ETG turbulence and the associated anomalous electron heat transport. Hence, one cannot conclude from the simulations reported here, nor those reported in Ref. [Lin] that ETG turbulence can be eliminated as a candidate for producing significant electron heat transport in experimental plasmas.

In summary, we have resolved the dispute between Ref. [Dorland, 2000; Jenko, 2000; Jenko, 2002] and Ref. [Lin, 2004; Lin, 2004a; Lin, 2005] regarding the behavior of Cyclone base-case-like ETG turbulence in favor of [Dorland, 2000; Jenko, 2000; Jenko, 2002].

Acknowledgements

We gratefully acknowledge discussions with Bill Dorland and Frank Jenko regarding their continuum ETG turbulence simulations; Bruce Cohen for his interest, advice, and careful editing; and W.W. Lee and Z. Lin for their contributions to increasing interest in

the subject matter addressed here. This work was performed under the auspices of the U.S. Department of Energy by UC, Lawrence Livermore National Laboratory under contract No. W-7405-ENG-48 and by Princeton Plasma Physics Laboratory under contract No. DE-AC02-76CH03073. The simulations described here made use of resources at the National Energy Research Supercomputer Center under Department of Energy Contract No. DE-AC03-76SF00098.

References

[Birdsall, 1985] C.K. Birdsall and A.B. Landgon, *Plasma Physics via Computer Simulation*, (McGraw-Hill, New York, 1985).

[Candy, 2004] J. Candy, R.E. Waltz, and W. Dorland, Phys. Plasmas **11**, L25 (May, 2004).

[Dimits, 1988] A.M. Dimits, Ph.D. thesis, Princeton University, 1988.

[Dimits, 1993] A.M. Dimits and W.W. Lee, JCP, (1993).

[Dimits, 1996] A.M. Dimits, , T.J. Williams, J.A. Byers, and B.I. Cohen, PRL **77**, 71 (1996).

[Dimits, 2000] A.M. Dimits, G. Bateman, M.A. beer, B.I. Cohen, W. Dorland, G.W. Hammett, C. Kim, J.E. Kinsey, M. Kotschenreuther, A.H. Kritz, L.L. Lao, J. Mandrekas, W.M. Nevins, S.E. Parker, A.J. Redd, D.E. Shumaker, R. Sydora, and J. Weiland, Phys. Plasmas **7**, 969 (March, 2000).

[Dorland, 2000] W. Dorland, F. Jenko, M Kotschenreuther, and B.N. Rogers, PRL **85**, 5579 (December, 2000).

[Hammett, 2005] G. Hammett, in preparation.

[Jenko, 2000] F. Jenko, W. Dorland, M. Kotschenreuther and B.N. Rogers, Phys. Plasmas **7**, 1904 (May, 2000).

[Jenko, 2002] Jenko and Dorland, PRL **89**, 225001 (November, 2002).

[Kotschenreuther, 1993] M. Kotschenreuther et al, Proceedings of the 14th International Conference on Plasma Physics and Controlled Nuclear Fusion, 1992 (IAEA, Vienna, 1993), Vol 2, p. 11.

[Krommes, 1993] J.A. Krommes, Phys. Fluids B5, 1066 (April, 1993).

[Langdon, 1979] A. Bruce Langdon, Phys. Fluids, (1979)

[Lee, 1983] W.W. Lee, Phys. Fluids, (1983).

[Lee, 1988] W.W. Lee and W. Tang, Phys. Fluids **31**, 612 (1988).

[Lee, 2004] W.W. Lee, *Steady State Global Simulations of Microturbulence*,Bull. Am. Phys. Soc. (November, 2004). See http://www.aps.org/meet/DPP04/baps/index.html .

[Lin, 2004] Z. Lin, L. Chen, Y. Nishimura, H. Qu, T.S. Hahm, J.L.V. Lewandowski, G. Rewoldt, W.X. Wang, P.H. Diamond, C. Holland, F. Zonka, and Y. Li, *Electron Thermal transport in Tokamaks: ETG or TEM Turbulence?* Fusion Energy 2004 (Proc. 20th Fusion Energy Conference, IAEA, 2004) paper TH8_4.

[Lin, 2004a] Z. Lin, *On Structures in Electron Temperature Gradient Turbulence*, Bull. Am. Phys. Soc. (November, 2004). See http://www.aps.org/meet/DPP04/baps/index.html .

[Lin 2005] Z. Lin, L. Chen, and F. Zonca, Phys. Plasmas **12**, 056125 (May, 2005).

[Parker, 1993] S.E. Parker and W.W. Lee, Phys. Fluids B **5**, 77 (1993).

[Roache, 1998] P.J. Roache, *Verification and Validation in Computational Science and Engineering*, (Hermosa Publishers, Albuquerque, NM, 1998).

[Waltz, 2002] R.E. Waltz, Fusion Energy 2002 (Proc. 19th Fusion Energy Conference, Lyon, 2002), TH1-D.